HHS Public Access

Author manuscript

Nano Lett. Author manuscript; available in PMC 2019 September 12.

Published in final edited form as:

Nano Lett. 2018 September 12; 18(9): 5702–5708. doi:10.1021/acs.nanolett.8b02298.

Ultrasensitive graphene optoelectronic probes for recording electrical activities of individual synapses

Rui Wang[1,+], **Mingjian Shi**[2,+], **Bryson Brewer**[3,+], **Lijie Yang**[3,+], **Yuchen Zhang**[4], **Donna J. Webb**[2,5,++], **Deyu Li**[3,*], and **Ya-Qiong Xu**[1,4,*]

[1]Department of Physics and Astronomy, Vanderbilt University, Nashville, TN 37212, USA

[2]Department of Biological Science and Vanderbilt Kennedy Center for Research on Human Development, Vanderbilt University, Nashville, TN 37212, USA

[3]Department of Mechanical Engineering, Vanderbilt University, Nashville, TN 37212, USA

[4]Department of Electrical Engineering and Computer Science, Vanderbilt University, Nashville, TN 37212, USA

[5]Department of Cancer Biology, Vanderbilt University, Nashville, TN 37212, USA

Abstract

The complex neuronal circuitry connected by sub-micron synapses in our brain calls for technologies that can map neural networks with ultrahigh spatiotemporal resolution to decipher the underlying mechanisms for multiple aspects of neuroscience. Here we show that through combining graphene transistor arrays with scanning photocurrent microscopy, we can detect the electrical activities of individual synapses of primary hippocampal neurons. Through measuring the local conductance change of graphene optoelectronic probes directly underneath neuronal processes, we are able to estimate millivolt extracellular potential variations of individual synapses during depolarization. The ultrafast nature of graphene photocurrent response allows for decoding of activity patterns of individual synapses with a sub-millisecond temporal resolution. This new neurotechnology provides promising potentials for recording of electrophysiological outcomes of individual synapses in neural networks.

Keywords

graphene; photocurrent; transistor; synapse; hippocampal neuron

The central nervous system in human brains is composed of billions of neurons with trillions of dendritic spines and synapses. Interestingly, emerging data indicate that individual synaptic connections are unique and can display different activities;[1–3] thus, it is important to correlate the functional connectivity map of neural networks with the physiological or pathological behaviors of individual spines and synapses. This requires recording of the electrical activities of individual synapses/spines with high spatiotemporal resolution and

*Correspondence to: yaqiong.xu@vanderbilt.edu and deyu.li@vanderbilt.edu.
+These authors contributed equally to this work.
++Deceased.

electrical sensitivity, which poses significant challenges to neurotechnology. Existing methodologies for measuring the electrical activity of neurons fall into three main categories: optical imaging, patch-clamp recording, and microelectrode arrays (MEAs). Optical imaging based on voltage- and calcium-sensitive dyes offers high throughput in terms of simultaneous sampling of axons and dendrites of multiple neurons,[4] but suffers from a trade-off between the electrical sensitivity and temporal resolution.[5] Patch-clamp recording can provide an accurate readout of the entire dynamic range of voltages generated by cells with pico-ampere-current sensitivity and sub-millisecond temporal resolution.[6] However, classic approaches are invasive and require the use of bulky micromanipulators, limiting their use to snapshots of few neurons over limited amount of time. In contrast, cell-non-invasive MEAs enable simultaneous stimulation and recording of large populations of neurons for days and months without mechanical damage.[7] To improve the electrical coupling between neurons and electrodes, penetrating MEAs have been developed to improve the stimulation effectiveness and recording qualities.[8–9] Another way is to use the gate electrode of a field-effect transistor (FET) as the sensing element.[10–13] Still, it is challenging to reduce transistor/electrode size for recording of electrical activity of individual synapses and spines with high electrical sensitivity. Therefore, it is crucial to develop a sensing scheme to study electrical activities of individual synapses with high spatial accuracy and high electrical sensitivity.

Recently, graphene has gained tremendous attention due to its extraordinary electrical, mechanical, and optical properties. A unique advantage of graphene is that its entire volume is exposed to the environment, which maximizes its sensitivity to local electrochemical potential change. For example, graphene FETs are capable of detecting individual gas molecules, owing to its high surface-area-to-volume ratio and high electron mobility.[14–17] The high electron mobility also enables graphene FETs to operate up to 500 GHz,[18–19] leading to high temporal resolution (pico-second). Importantly, monolayer graphene transmits more than 97% of incident light,[20] making it compatible with optical imaging. All these unique properties, together with the demonstrated excellent biocompatibility,[21–29] make graphene an ideal candidate to address the challenge of sensing the electrical activities of individual synapses in neural networks.

Through directly culturing primary hippocampal neurons on graphene FET arrays and probing the local electrical conductance change at the graphene-synapse junctions via scanning photocurrent microscopy, we demonstrate the capability of recording the electrical activities of individual synapses (~800 nm, determined by the diffraction-limit of a laser spot). The ultrafast nature of graphene photocurrent response allows decoding a single waveform that may coincide with action potentials from the bursts of individual synapses and spines with a sub-millisecond temporal resolution. Importantly, we show that the 2D nature of graphene enables recording of the millivolt extracellular potential changes of randomly-distributed individual synapses/spines.

In our studies, we integrated graphene transistor arrays with a microfluidic neuron-glia co-culture platform (Fig. 1A) that could dynamically image spine and synapse formation through separately transfecting two populations of neurons with pre- and post-synaptic markers.[30–31] High-quality graphene was synthesized via a standard chemical vapor

deposition method[32–33] and transferred onto 170 μm thick transparent coverslips with pre-patterned gold electrodes,[34] forming graphene FETs that were then aligned and bonded with the top microfluidic polydimethylsiloxane (PDMS) structure. Direct transfer of graphene prevents contamination during device fabrication to achieve ultraclean carbon surfaces; and the glass coverslip substrate allows for scanning photocurrent measurements from the lower surface to detect the local photoconductance of graphene (Fig. 1B) via an oil immersion objective to achieve a diffraction limit of ~800 nm.[35] We used Raman spectroscopy to inspect the quality and thickness of graphene on a coverslip with a 532 nm laser. As shown in Fig. S1A, the 2D peak has a symmetric shape and the 2D-to-G intensity ratio is about 2, indicating that the as-grown graphene has a monolayer structure.[36–37] Next, we tested the electrical response of the graphene transistors in our microfluidic chambers by including a large gold pad that acted as an electrolyte gate to modulate the electrochemical environment of graphene. Gate-dependent conductance measurement of a typical graphene transistor displayed p-type semiconducting characteristics (Fig. S1D), consistent with previous reports of electrolyte-gated graphene transistors.[38–39]

To probe electrical activities of neuronal processes with these graphene FETs, we co-cultured primary embryonic hippocampal neurons with glia to maintain healthy cultures that make direct contact with graphene transistors. In our microfluidic platforms, the graphene transistors were positioned underneath a middle channel that was between two inner chambers with neurons (Fig. 1A and 1C). The neurons in these two chambers were separately transfected with plasmid constructs expressing either mCherry-synaptophysin (red, Fig. 1D), a pre-synaptic marker, or mCerulean (blue, Fig. 1E), which marks dendritic spines containing post-synaptic densities. Glia were loaded into the two outer chambers to support the growth and differentiation of the hippocampal neurons. The mid-channel and cell chambers are separated by PDMS valve barriers with microgrooves underneath them, which can be controlled to be either closed or open by the hydraulic pressure in a control chamber constructed on top of the cell culture layer. In the closed position, the valve barriers completely isolated the chambers for separate culture or treatment of each cell population.[40] When the valve barriers were in the open position, the microgrooves connected the chambers, allowing for interactions and communication between cells in different chambers. After 8 to 12 days in culture, neuronal processes extended toward the adjacent chambers and contacted each other in the mid-channel. We then used fluorescence microscopy to visualize synaptic contacts between mCherry-synaptophysin (red) and mCerulean (blue) (Fig. 1F–1H). In addition, GFP-GCaMP6s (a fluorescence Ca^{2+} indicator, green, Fig. 1I) was also used to characterize synaptic activities.

After locating individual spines and synapses using optical and fluorescence microscopy (Fig. 2A–2D), we measured the photocurrent response of the graphene transistor underneath these spines and synapses (Fig. 2E). Here the neuronal activity initiated action potentials along their axons that could change local electrochemical environments, influencing the local charge carrier concentration of graphene and thus modifying its local energy band diagram (Fig. 2F). When a diffraction-limited laser spot (λ = 785 nm) scanned over a graphene transistor through a piezo-controlled mirror with nanometer-scale spatial resolution, a photocurrent signal occurred wherever the graphene energy band bended; the built-in electric field separated photo-excited electron and hole pairs (EHPs), and thus

produced an electric current.[41] We extracted band diagrams (E_F–E_{Dirac}) through numerical integration of photocurrent profiles.[39, 41] The electron energy of graphene follows a linear dispersion near the Dirac point, with a Fermi energy of $E_F - E_{Dirac} \approx \hbar v_F \sqrt{\pi n}$, where $v_F \approx 10^6 m/s$ is the Fermi velocity and n is the charge carrier concentration.[42] We then calculated the local charge ($Q = ne$) of graphene from photocurrent data and derived a local potential ($V = Q/C$), where C is a combination of the electrostatic capacitance between the graphene and a synapse/spine and the quantum capacitance of the graphene. The minimum quantum capacitance $C_{Q,min}$ is about $6.5 \mu F/cm^2$,[43] and the double layer capacitance of the electrolyte C_i is approximately $20 \mu F/cm^2$.[44] Thus, the total capacitance C is ~$4.9 \mu F/cm^2$. If we simply use the graphene transistor without the scanning photocurrent scheme as our sensing approach, then we face a major challenge that the local ion concentration change has to provide enough charge to affect the conductance of the entire graphene membrane between the source and drain electrodes. In contrast, introducing scanning photocurrent microscopy allows for probing of the local conductance of a small area of graphene piece, which corresponds to a region of the diffraction-limited laser spot of about $0.8 \mu m$ in diameter. For such a small piece of graphene as an optoelectronic probe, the maximum corresponding capacitance is ~$25 fF$, leading to ultrahigh electrical sensitivity.

Our results show remarkable photocurrent signals generated at spots where spines and synapses were located (Fig. 2E), indicating that our approach can be used to detect electrical activities of individual synapses and spines with submicron spatial resolution. We then compared our photocurrent scheme with traditional fluorescence-based imaging approaches. The local potential of neuronal membranes increased upon high-K^+ stimulation, which led to changes in both the fluorescence intensity of GFP-GCaMP6s (Fig. 2G–2H) and in the photocurrent response of graphene-synapse junctions (Fig. 2I–2K) as we switched between high-K^+ and low-K^+ media in the chamber (the total ionic concentration was kept as a constant), underscoring the validity of our approach. Interestingly, even though the photocurrent measurements follow the same general trend, the electrical responses of individual synapses vary from synapse-to-synapse during depolarization (Fig. 2H), which is interesting and will be further explored. Note that after two depolarization cycles the fluorescence signal was photobleached, but the electrical response of individual spines and synapses could still be detected by photocurrent measurements. Importantly, we could derive the local extracellular membrane potential changes (~2 mV) during the depolarization from our photocurrent measurements (for details, see SI).

To examine the temporal resolution of graphene optoelectronic probes, we studied chemically-evoked bursts by raising the extracellular K^+ concentration from 4 mM to 60 mM. In our experiments, DIC and fluorescence images were used to identify a synaptic contact (Fig. 3A–3F), and the laser beam was then focused on the corresponding graphene-synapse junction to collect the photocurrent responses every 50 μs to record the local electrical activity at the junction. As shown in Fig 3H, bursts occurred when the extracellular K^+ concentration increased to 60 mM; and these bursts disappeared when the extracellular K^+ concentration was reduced to 4 mM. We also found that no burst was observed in the second and third cycles, which could be due to the cytotoxic effect of high-K^+ concentration.[45–48] The high electrical sensitivity and temporal resolution of graphene optoelectronic

probes also allowed us to decode the detailed spontaneous waveform of each burst. As shown in Fig. 3I, the burst has a waveform with a width about 2–3 ms, whose shape is similar to an action potential with a maximum extracellular potential change of ~14 mV (for details, see SI). Interestingly, synapses responded differently in the high-K^+ concentration media. For example, chemically-evoked bursts of another graphene-synapse junction, which was identified by DIC and photocurrent images (Fig. 4A and 4B), were observed at regular intervals with a frequency of 0.2 Hz (Fig. 4C). After the extracellular K^+ concentration was reduced to 4 mM, the bursts disappeared. We also found that the burst intensity and frequency decreased in the second 90 mM cycle, while no burst was observed in the third and fourth cycles. Close examination of the bursts reveals that each burst includes a series of peaks with widths of 2–10 ms, which is likely related to action potentials or postsynaptic responses.

In conclusion, by combining graphene transistor arrays with scanning photocurrent microscopy, we created a unique approach that can record electrical activities of individual synapses with a sub-millisecond temporal resolution and high electrical sensitivity. We demonstrated the power of this sensing scheme by probing the electrical responses of individual spines and synapses in primary embryonic hippocampal neuron cultures at rest and during depolarization. Importantly, we were able to decode detailed waveforms of the chemically-evoked bursts of individual synapses during depolarization. Furthermore, the 2D nature of graphene allows recording of randomly-distributed individual synapses/spines. As such, this new neurotechnology provides the potential capability of large-area mapping with a high spatiotemporal resolution to explore neural networks with detailed information of activities and signal events at a single-synapse level. This technology should also be able to probe many other cellular systems involving cell-cell interactions through electrical signaling.

Supplementary Material

Refer to Web version on PubMed Central for supplementary material.

Acknowledgements

This paper is dedicated to Dr. D.J. Webb who passed away on May 15, 2017. This work was supported by the National Institutes of Health (1R01EY027729, 1R21EY026176, and 1R21NS095323) and the National Science Foundation (ECCS-1055852 & 1810088, CBET-1264982, and BIO-1450897). Device Fabrication was conducted at the Center for Nanophase Materials Sciences, which is a DOE Office of Science User Facility.

REFERENCES AND NOTES

1. Trommershauser J; Schneggenburger R; Zippelius A; Neher E, Heterogeneous presynaptic release probabilities: functional relevance for short-term plasticity. Biophys J 2003, 84 (3), 1563–1579. [PubMed: 12609861]
2. Reyes A; Lujan R; Rozov A; Burnashev N; Somogyi P; Sakmann B, Target-cell-specific facilitation and depression in neocortical circuits. Nat Neurosci 1998, 1 (4), 279–285. [PubMed: 10195160]
3. Markram H; Wang Y; Tsodyks M, Differential signaling via the same axon of neocortical pyramidal neurons. Proc Natl Acad Sci U S A 1998, 95 (9), 5323–5328. [PubMed: 9560274]

4. Chen TW; Wardill TJ; Sun Y; Pulver SR; Renninger SL; Baohan A; Schreiter ER; Kerr RA; Orger MB; Jayaraman V; Looger LL; Svoboda K; Kim DS, Ultrasensitive fluorescent proteins for imaging neuronal activity. Nature 2013, 499 (7458), 295–300. [PubMed: 23868258]

5. Carlson GC; Coulter DA, In vitro functional imaging in brain slices using fast voltage-sensitive dye imaging combined with whole-cell patch recording. Nat Protoc 2008, 3 (2), 249–255. [PubMed: 18274527]

6. Novak P; Gorelik J; Vivekananda U; Shevchuk Andrew I.; Ermolyuk Yaroslav S.; Bailey Russell J.; Bushby Andrew J.; Moss Guy W. J.; Rusakov Dmitri A.; Klenerman D; Kullmann Dimitri M.; Volynski Kirill E.; Korchev Yuri E., Nanoscale-Targeted Patch-Clamp Recordings of Functional Presynaptic Ion Channels. Neuron 2013, 79 (6), 1067–1077. [PubMed: 24050398]

7. Spira ME; Hai A, Multi-electrode array technologies for neuroscience and cardiology. Nat Nanotechnol 2013, 8 (2), 83–94. [PubMed: 23380931]

8. Normann RA; Fernandez E, Clinical applications of penetrating neural interfaces and Utah Electrode Array technologies. J Neural Eng 2016, 13 (6), 061003. [PubMed: 27762237]

9. Patel PR; Zhang HN; Robbins MT; Nofar JB; Marshall SP; Kobylarek MJ; Kozai TDY; Kotov NA; Chestek CA, Chronic in vivo stability assessment of carbon fiber microelectrode arrays. J Neural Eng 2016, 13 (6), 066002. [PubMed: 27705958]

10. Hutzler M; Lambacher A; Eversmann B; Jenkner M; Thewes R; Fromherz P, High-resolution multitransistor array recording of electrical field potentials in cultured brain slices. J Neurophysiol 2006, 96 (3), 1638–1645. [PubMed: 16687618]

11. Qing Q; Pal SK; Tian B; Duan X; Timko BP; Cohen-Karni T; Murthy VN; Lieber CM, Nanowire transistor arrays for mapping neural circuits in acute brain slices. Proc Natl Acad Sci U S A 2010, 107 (5), 1882–1887. [PubMed: 20133836]

12. Patolsky F; Timko BP; Yu G; Fang Y; Greytak AB; Zheng G; Lieber CM, Detection, stimulation, and inhibition of neuronal signals with high-density nanowire transistor arrays. Science 2006, 313 (5790), 1100–1104. [PubMed: 16931757]

13. Tian B; Liu J; Dvir T; Jin L; Tsui JH; Qing Q; Suo Z; Langer R; Kohane DS; Lieber CM, Macroporous nanowire nanoelectronic scaffolds for synthetic tissues. Nat Mater 2012, 11 (11), 986–994. [PubMed: 22922448]

14. Geim AK, Graphene: Status and Prospects. Science 2009, 324 (5934), 1530–1534. [PubMed: 19541989]

15. Novoselov KS; Geim AK; Morozov S; Jiang D; Zhang Y; Dubonos S. a.; Grigorieva I; Firsov A, Electric field effect in atomically thin carbon films. science 2004, 306 (5696), 666–669. [PubMed: 15499015]

16. Novoselov KS; Jiang D; Schedin F; Booth TJ; Khotkevich VV; Morozov SV; Geim AK, Two-dimensional atomic crystals. Proceedings of the National Academy of Sciences of the United States of America 2005, 102 (30), 10451–10453. [PubMed: 16027370]

17. Schedin F; Geim AK; Morozov SV; Hill EW; Blake P; Katsnelson MI; Novoselov KS, Detection of individual gas molecules adsorbed on graphene. Nat Mater 2007, 6 (9), 652–655. [PubMed: 17660825]

18. Lin YM; Dimitrakopoulos C; Jenkins KA; Farmer DB; Chiu HY; Grill A; Avouris P, 100-GHz Transistors from Wafer-Scale Epitaxial Graphene. Science 2010, 327 (5966), 662–662. [PubMed: 20133565]

19. Xia F; Mueller T; Lin Y.-m.; Valdes-Garcia A; Avouris P, Ultrafast graphene photodetector. Nat Nano 2009, 4 (12), 839–843.

20. Bae S; Kim H; Lee Y; Xu XF; Park JS; Zheng Y; Balakrishnan J; Lei T; Kim HR; Song YI; Kim YJ; Kim KS; Ozyilmaz B; Ahn JH; Hong BH; Iijima S, Roll-to-roll production of 30-inch graphene films for transparent electrodes. Nature Nanotechnology 2010, 5 (8), 574–578.

21. Sahni D; Jea A; Mata JA; Marcano DC; Sivaganesan A; Berlin JM; Tatsui CE; Sun ZZ; Luerssen TG; Meng SY; Kent TA; Tour JM, Biocompatibility of pristine graphene for neuronal interface Laboratory investigation. J Neurosurg-Pediatr 2013, 11 (5), 575–583. [PubMed: 23473006]

22. Kuzum D; Takano H; Shim E; Reed JC; Juul H; Richardson AG; de Vries J; Bink H; Dichter MA; Lucas TH; Coulter DA; Cubukcu E; Litt B, Transparent and flexible low noise graphene electrodes

for simultaneous electrophysiology and neuroimaging. Nat Commun 2014, 5, 5259. [PubMed: 25327632]

23. Park DW; Schendel AA; Mikael S; Brodnick SK; Richner TJ; Ness JP; Hayat MR; Atry F; Frye ST; Pashaie R; Thongpang S; Ma ZQ; Williams JC, Graphene-based carbon-layered electrode array technology for neural imaging and optogenetic applications. Nat Commun 2014, 5, 5258. [PubMed: 25327513]
24. Chen H; Muller MB; Gilmore KJ; Wallace GG; Li D, Mechanically strong, electrically conductive, and biocompatible graphene paper. Advanced Materials 2008, 20 (18), 3557–3561.
25. Li N; Zhang Q; Gao S; Song Q; Huang R; Wang L; Liu LW; Dai JW; Tang ML; Cheng GS, Three-dimensional graphene foam as a biocompatible and conductive scaffold for neural stem cells. Sci Rep 2013, 3, 1604. [PubMed: 23549373]
26. Li N; Zhang XM; Song Q; Su RG; Zhang Q; Kong T; Liu LW; Jin G; Tang ML; Cheng GS, The promotion of neurite sprouting and outgrowth of mouse hippocampal cells in culture by graphene substrates. Biomaterials 2011, 32 (35), 9374–9382. [PubMed: 21903256]
27. Park SY; Park J; Sim SH; Sung MG; Kim KS; Hong BH; Hong S, Enhanced differentiation of human neural stem cells into neurons on graphene. Advanced Healthcare Materials 2011, 23 (36), H263–H267.
28. Fischer RA; Zhang Y; Risner ML; Li D; Xu Y; Sappington RM, Impact of Graphene on the Efficacy of Neuron Culture Substrates. Advanced Healthcare Materials 2018, 1701290.
29. Kitko KE; Hong T; Lazarenko RM; Ying D; Xu YQ; Zhang Q, Membrane cholesterol mediates the cellular effects of monolayer graphene substrates. Nat Commun 2018, 9, 796. [PubMed: 29476054]
30. Gao Y; Majumdar D; Jovanovic B; Shaifer C; Lin PC; Zijlstra A; Webb DJ; Li D, A versatile valve-enabled microfluidic cell co-culture platform and demonstration of its applications to neurobiology and cancer biology. Biomed Microdevices 2011, 13 (3), 539–548. [PubMed: 21424383]
31. Majumdar D; Gao YD; Li DY; Webb DJ, Co-culture of neurons and glia in a novel microfluidic platform. J Neurosci Meth 2011, 196 (1), 38–44.
32. Li X; Cai W; An J; Kim S; Nah J; Yang D; Piner R; Velamakanni A; Jung I; Tutuc E, Large-area synthesis of high-quality and uniform graphene films on copper foils. Science 2009, 324 (5932), 1312–1314. [PubMed: 19423775]
33. Wang R; Hong T; Xu YQ, Ultrathin Single-Walled Carbon Nanotube Network Framed Graphene Hybrids. Acs Appl Mater Inter 2015, 7 (9), 5233–5238.
34. Hong T; Cao Y; Ying D; Xu Y-Q, Thermal and optical properties of freestanding flat and stacked single-layer graphene in aqueous media. Appl Phys Lett 2014, 104 (22), 223102.
35. Xu YQ; Barnard A; McEuen PL, Bending and Twisting of Suspended Single-Walled Carbon Nanotubes in Solution. Nano Letters 2009, 9 (4), 1609–1614. [PubMed: 19351193]
36. Ferrari AC; Basko DM, Raman spectroscopy as a versatile tool for studying the properties of graphene. Nature Nanotechnology 2013, 8 (4), 235–246.
37. Cao YH; Flores RL; Xu YQ, Curling graphene ribbons through thermal annealing. Appl Phys Lett 2013, 103 (18), 183103.
38. Cohen-Karni T; Qing Q; Li Q; Fang Y; Lieber CM, Graphene and nanowire transistors for cellular interfaces and electrical recording. Nano Lett 2010, 10 (3), 1098–1102. [PubMed: 20136098]
39. Zhang Y; Dodson KH; Fischer R; Wang R; Li D; Sappington RM; Xu Y-Q, Probing electrical signals in the retina via graphene-integrated microfluidic platforms. Nanoscale 2016, 8 (45), 19043–19049. [PubMed: 27812594]
40. Shi MJ; Majumdar D; Gao YD; Brewer BM; Goodwin CR; McLean JA; Lib D; Webb DJ, Glia co-culture with neurons in microfluidic platforms promotes the formation and stabilization of synaptic contacts. Lab on a Chip 2013, 13 (15), 3008–3021. [PubMed: 23736663]
41. Mueller T; Xia F; Freitag M; Tsang J; Avouris P, Role of contacts in graphene transistors: A scanning photocurrent study. Phys Rev B 2009, 79 (24), 245430.
42. Das Sarma S; Adam S; Hwang EH; Rossi E, Electronic transport in two-dimensional graphene. Rev Mod Phys 2011, 83 (2), 407–470.

43. Xia JL; Chen F; Li JH; Tao NJ, Measurement of the quantum capacitance of graphene. Nature Nanotechnology 2009, 4 (8), 505–509.

44. Randin JP; Yeager E, Differential Capacitance Study of Stress/Annealed Pyrolytic Graphite Electrodes. Journal of the Electrochemical Society 1971, 118 (5), 711–714.

45. Ramnath RR; Strange K; Rosenberg PA, Neuronal Injury Evoked by Depolarizing Agents in Rat Cortical Cultures. Neuroscience 1992, 51 (4), 931–939. [PubMed: 1362603]

46. Schramm M; Eimerl S; Costa E, Serum and Depolarizing Agents Cause Acute Neurotoxicity in Cultured Cerebellar Granule Cells - Role of the Glutamate Receptor Responsive to N-Methyl-D-Aspartate. Proceedings of the National Academy of Sciences of the United States of America 1990, 87 (3), 1193–1197. [PubMed: 2153974]

47. Takahashi M; Liou SY; Kunihara M, Ca2+-Dependent and Cl--Dependent, Nmda Receptor-Mediated Neuronal Death Induced by Depolarization in Rat Hippocampal Organotypic Cultures. Brain Research 1995, 675 (1–2), 249–256. [PubMed: 7796136]

48. Rothman SM, The Neurotoxicity of Excitatory Amino-Acids Is Produced by Passive Chloride Influx. Journal of Neuroscience 1985, 5 (6), 1483–1489. [PubMed: 3925091]

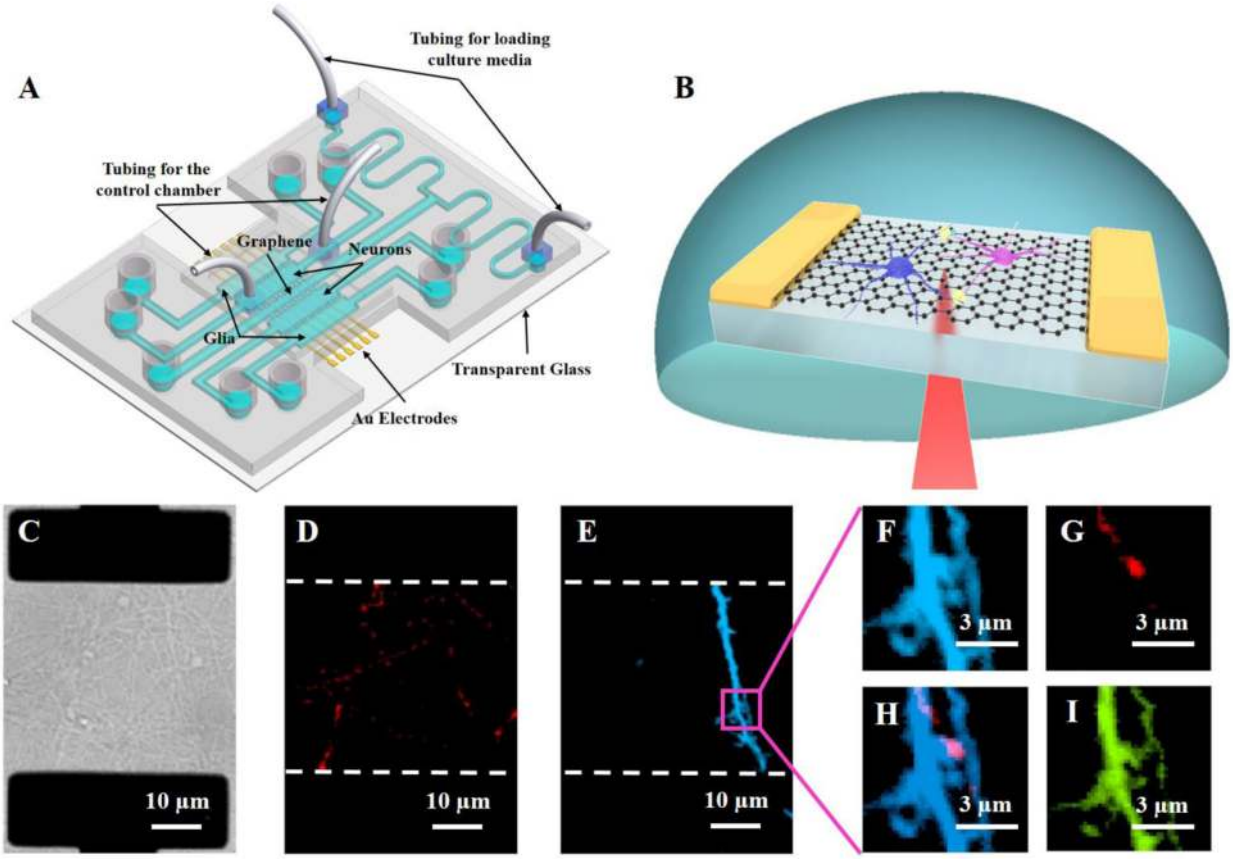

Fig. 1.

(A) Schematic of a four-chamber neuron-glia co-culture microfluidic device with integrated graphene transistors. **(B)** Schematic of scanning photocurrent measurements. A diffraction-limited laser spot passes through a transparent coverslip to scan over the graphene underneath neurons. **(C)** Differential interference contrast (DIC) of a graphene transistor underneath neural networks. The two black rectangles are opaque Au electrodes that are underneath the graphene membrane. Neurons, at day 5 in culture, were differentially transfected with **(D)** mCherry-synaptophysin (red) and **(E)** mCerulean (blue), maintained in co-culture with glia. Zoom-in fluorescence images of a magenta square region in Fig. 1E: **(F)** mCerulean (blue); **(G)** mCherry-synaptophysin (red); **(H)** overlay of mCerulean and mCherry-synaptophysin; and **(I)** GFP-GCaMP6s (green).

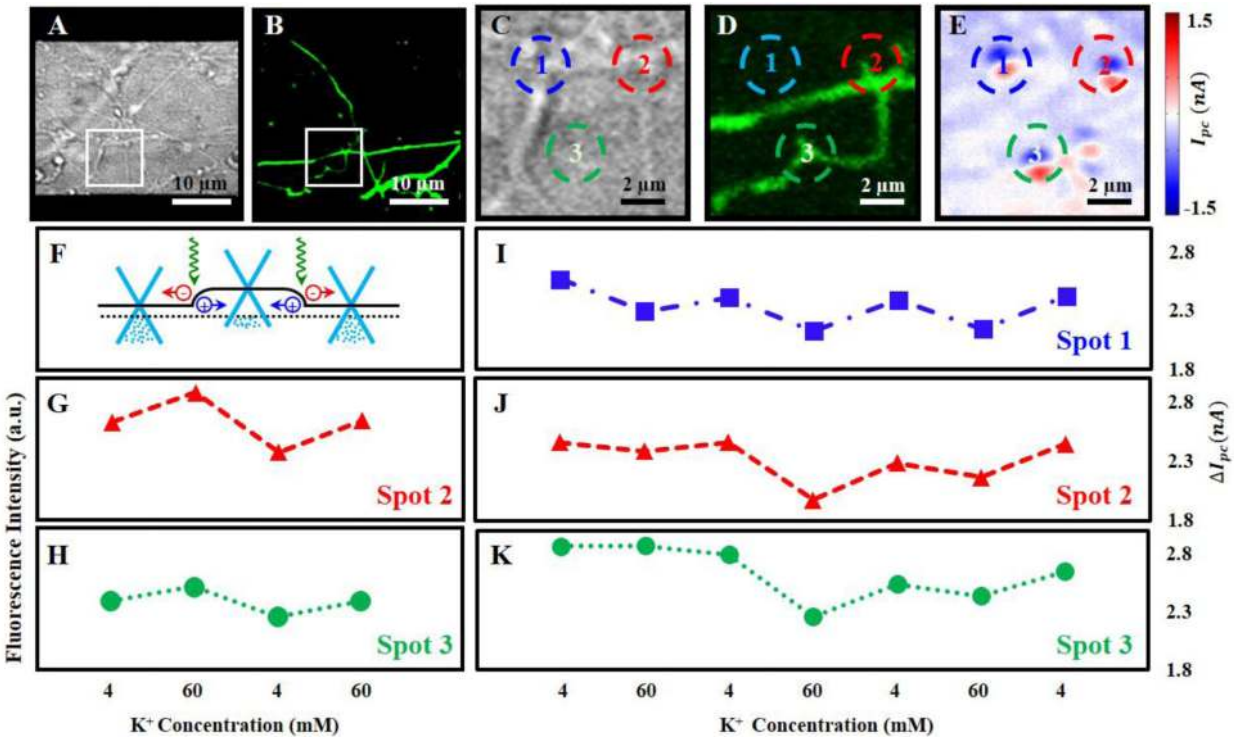

Fig. 2.

(A) DIC and **(B)** fluorescence (GFP-GCaMP6s, green) images of neurons, at day 8 in culture, on top of a graphene transistor. Zoom-in **(C)** DIC, **(D)** fluorescence, and **(E)** photocurrent images of the white square regions in Fig. 2A and 2B. Three synapses/spines are marked by blue, red, and green circles, respectively. **(F)** Schematic of band structures of graphene. The black dotted line denotes the Fermi level and the solid line shows the graphene band diagram. A local electrochemical potential change induced by a synapse/spine results in the local carrier concentration changes of graphene, leading to the graphene energy band bending and subsequent photocurrent generation. Fluorescence intensity changes when the neurons were exposed to 4 mM K^+, 60 mM K^+, 4 mM K^+, and 60 mM K^+, respectively. Red triangles and green spheres represent the fluorescence intensities of synapses/spines at spots two **(G)** and three **(H)** in Fig. 2D. Photocurrent responses of three graphene-synapse junctions upon three high-K^+ stimulation cycles (4–60–4–60–4–60–4). **(I)** Blue squares, **(J)** red triangles, and **(K)** green spheres represent the photocurrent responses of graphene-synapse junctions at spots with the corresponding color in Fig. 2E. ΔI_{pc} is the difference between the maximum (red) and minimum (blue) photocurrent response.

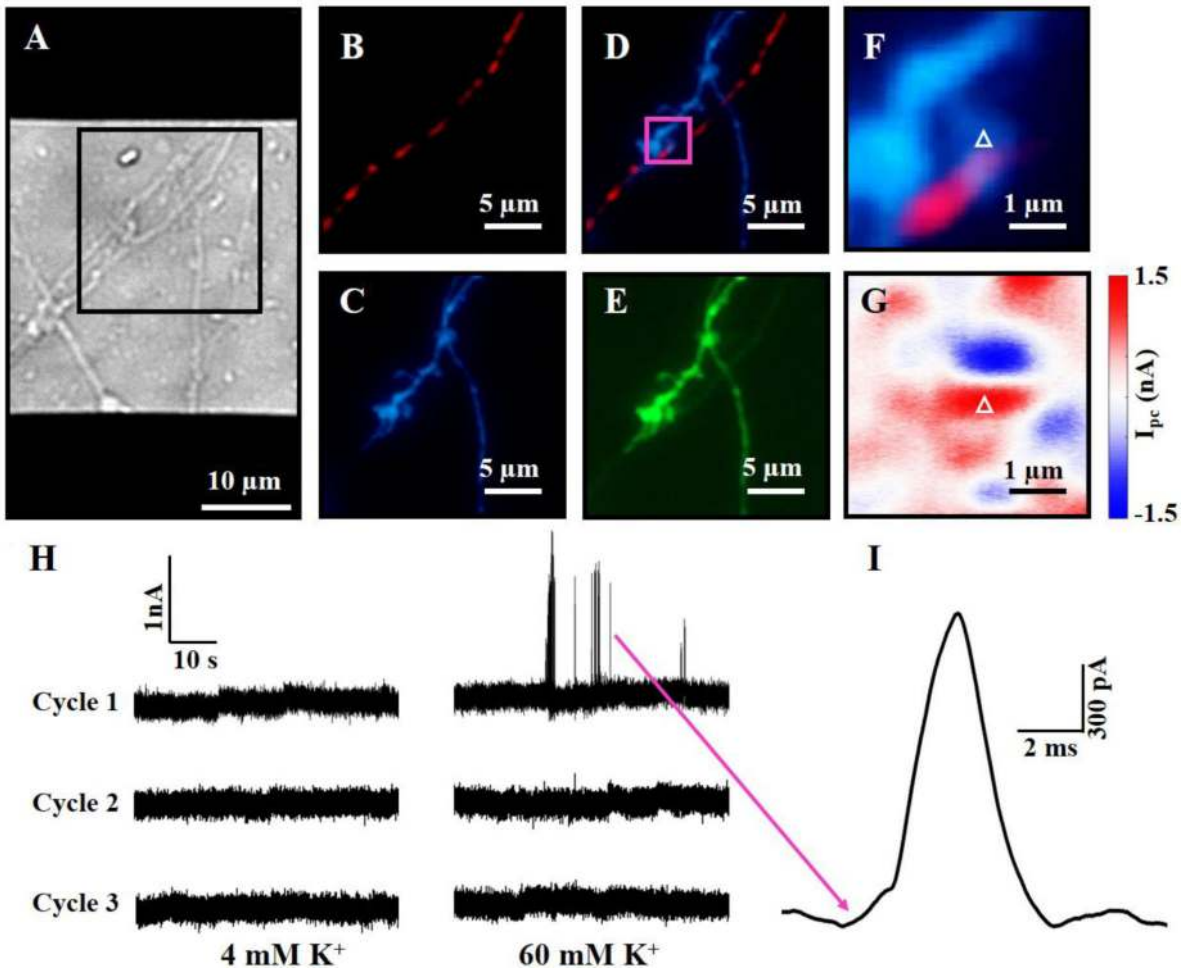

Fig. 3.

(**A**) DIC image of neurons, at day 9 in culture, atop a graphene transistor. Zoom-in fluorescence images of the black square region in Fig. 3A: **(B)** mCherry-synaptophysin (red); **(C)** mCerulean (blue); **(D)** overlay of mCerulean and mCherry-synaptophysin; and **(E)** GFP-GCaMP6s (green). Detailed fluorescence **(F)** and photocurrent **(G)** images of the magenta square region in Fig. 3D. **(H)** Photocurrent responses of a graphene-synapse junction (white triangles in Fig. 3F and 3G) upon three high-K^+ stimulation cycles (4–60–4–60–4–60). **(I)** Spontaneous waveform of a spike burst indicated by a magenta arrow in Fig. 3H.

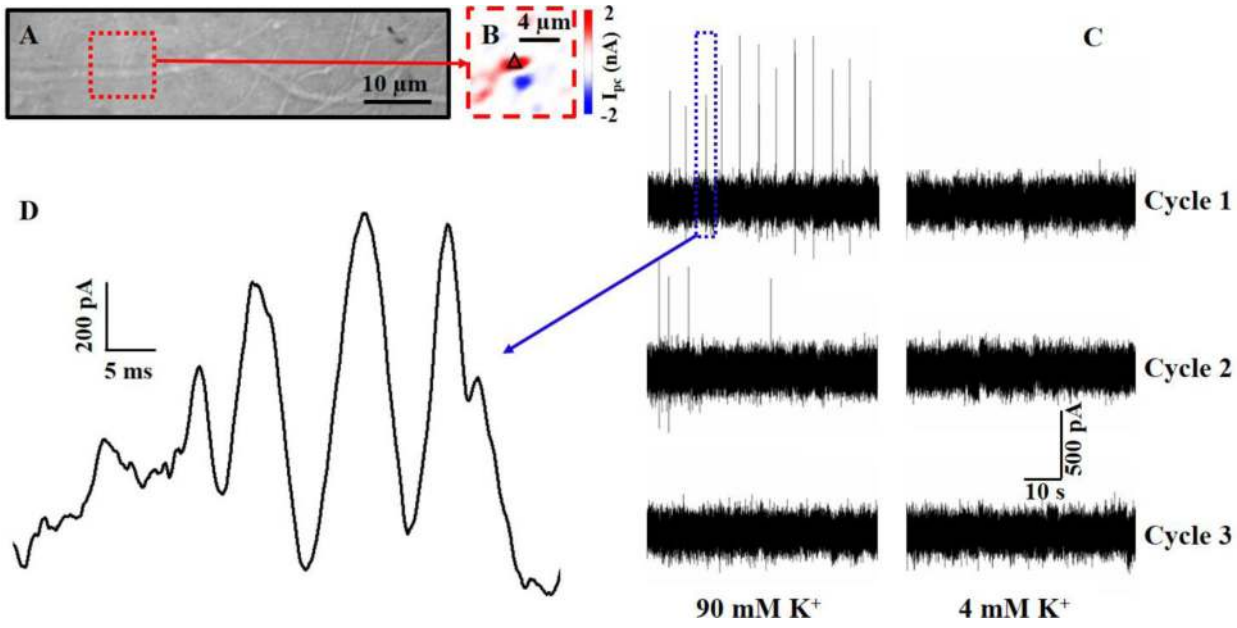

Fig. 4.

(**A**) DIC and **(B)** zoom-in photocurrent images of neurites, at day 8 in culture, on top of a graphene transistor. **(C)** Photocurrent responses of a graphene-synapse junction (a black triangle in Fig. 4B) upon three high-K^+ stimulation cycles (90–4–90–4–90–4). **(D)** Spontaneous waveform of a spike burst indicated by a blue dotted rectangular in Fig. 4C.